Bundling and Interdigitation of Adsorbed Thiolate Groups in Self-Assembled Nanocrystal Superlattices

Z. L. Wang*

School of Materials Science and Engineering, Georgia Institute of Technology, Atlanta, Georgia 30332-0245

S. A. Harfenist and R. L. Whetten

School of Physics, Georgia Institute of Technology, Atlanta, Georgia 30332

J. Bentley and N. D. Evans

Metals and Ceramics Division, Oak Ridge National Laboratory, Oak Ridge, Tennessee 37831-6376

Received: January 23, 1998; In Final Form: March 5, 1998

Self-assembling of nanocrystals involves organization of nanocrystals encapsulated by protective compact organic molecules into a crystalline material. The adsorbed molecules not only serve as the protection layer for the nanocrystals but also provide the dominant cohesive interactions (or "bonding") sustaining the nanocrystal superlattices. The length of the adsorbed molecules is a controllable parameter, making the ratio of particle size to interparticle distance an adjustable parameter that sensitively tunes the interparticle interaction/coupling and resulting collective properties. In this paper, bundling and interdigitation of thiolate molecules adsorbed on Ag nanocrystals are observed using the chemical imaging technique in energy-filtered transmission electron microscopy (EF-TEM) at a resolution of ∼2 nm. In these orientationally ordered, self-assembled Ag−nanocrystal superlattices, the bundling of the adsorbed molecules on the nanocrystal surfaces is the fundamental structural principle. A model consistent with the nanocrystal's morphology and the interdigitation of the adsorbed thiolates is proposed.

1. Introduction

Size- and shape-selected nanocrystals behave like molecular matter that functions as ideal building blocks for two- and three-dimensional cluster self-assembled superlattice structures.[1−4] Self-assembling involves organization of nanocrystals encapsulated within a protective compact organic coating into a crystalline material with translation and even orientation symmetry. This system contains ordering on two different length scales, atomic level and nanocrystal-assembly level; thus, the macroscopic properties of the nanocrystal superlattice (NCS) is determined not only by the properties of each individual particle but also by the interaction among nanocrystals interconnected and isolated by a monolayer of thin organic molecules. Furthermore, the length of the adsorbed molecules is a controllable parameter, rendering the ratio of particle size to interparticle distance adjustable,[5] possibly resulting in novel tunable structural, optical, and transport properties.[6]

The nanocrystal's adsorbed monolayer not only serves as the protective layer of the nanocrystals from agglomeration but also dominates the interparticle interactions, structure, and cohesion for the superlattice. Thus, the structural stability of NCSs is determined by the spatial distribution/directionality and connection of the adsorbed molecules on the surface. Although the structure of nanocrystals and NCSs can be determined by X-ray diffraction and transmission electron microscopy (TEM), direct imaging the passivation configuration of the surfactant is a challenge. In this paper, a new technique is introduced for directly imaging the thiolate distribution on nanocrystal surfaces. For truncated-octahedral (TO) silver nanocrystals of predominantly TO morphology, the adsorbed n-$CH_3(CH_2)_mS$ molecules are found to erectly bundle on the {100} and {111} surfaces of the nanocrystals and are highly directionally bunched, forming the interdigitative molecular bonding between the particles.

2. Compositional Imaging Using Energy-Filtered TEM

The compositional imaging mode of TEM is used to directly image the distribution of thiolate molecules on the surfaces of nanocrystals.[7] The energy filtered TEM (EF-TEM) forms images using the electrons that have excited a specific inelastic scattering process, such as the ionization of the carbon K shell electrons, so that the image contrast is directly proportional to the thickness-projected carbon concentration in the specimen. One of the energy-filtering methods in TEM is shown in Figure 1a, which uses an electron energy-loss spectroscopy (EELS) system attached to a TEM.[8] The system is composed of four components: TEM, EELS, energy-filtering system, and charge-coupled device (CCD) camera for digital data recording. The operation of the TEM is almost independent of the energy-filtering system because the energy-filtering occurs after the electron has passed through all of the lenses belonging to the TEM. The electrons are dispersed by the magnetic sectors in the EELS spectrometer; thus, electrons having different velocities (or energies) are focused onto different positions in the plane of the energy-selecting slit. The energy-selecting slit filters the electrons with a specific range of energy losses. A set of lenses are then arranged to redisperse the selected electrons to form

* To whom all correspondence should be addressed. E-mail: zhong.wang@mse.gatech.edu.

S1089-5647(98)00864-5 CCC: $15.00
Published on Web 04/04/1998

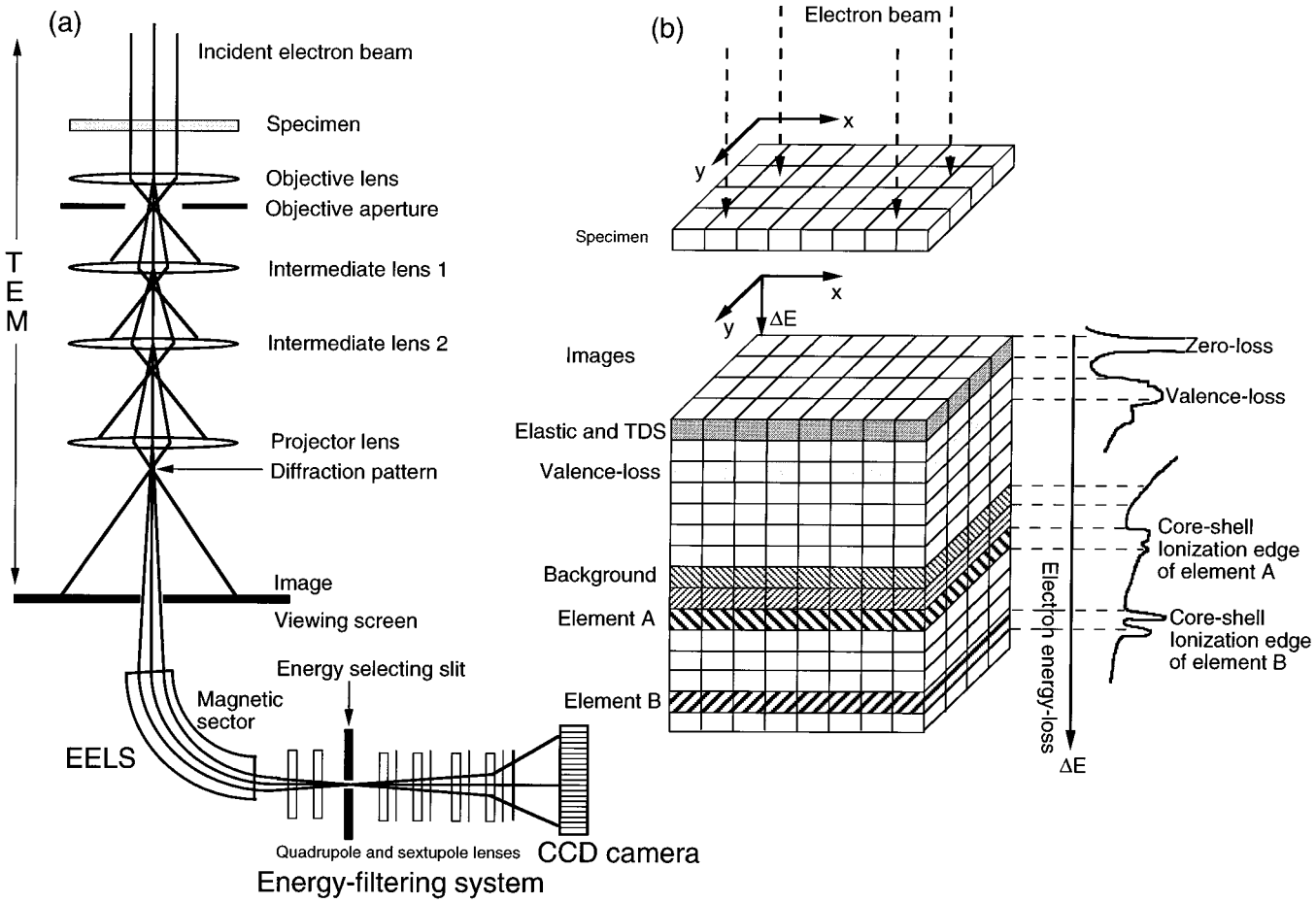

Figure 1. (a) Schematic diagram showing the energy-filtering system attached to a transmission electron microscope. (b) Schematic diagram showing energy-filtered electron imaging in TEM. The energy-selected electron images corresponding to different characteristic energy-loss features are shown, which can be used to extract useful structural and chemical information of the specimen. The conventional TEM image is recorded by integrating the electrons with different energy losses.

the image (or diffraction pattern). The final image/diffraction pattern is recorded digitally using the CCD camera.

With an energy filter, images (or diffraction patterns) formed by electrons with specific energy losses can be obtained, as illustrated in Figure 1b.[9] The energy-selected electron images can be simply illustrated using a three-dimensional data space, in which the *z*-axis represents the energy loss ΔE of the electrons and *x* and *y* are the real space coordinates of the two-dimensional image of the specimen. The inelastic scattering processes[10] observed in the EELS spectrum are schematically shown on the right-hand side of Figure 1b. The zero-loss peak is composed of elastically and phonon (or thermal diffusely) scattered electrons. Atomic inner-shell ionization edges can be employed to form composition-sensitive images. The background observed in the EELS spectrum is produced by scattering processes of multiple valence losses, electromagnetic radiation, and electron Compton scattering. To extract composition-sensitive images, the contribution made by these processes must be subtracted from the recorded data. Only the inner-shell ionization signal directly reflects the concentration of the corresponding element in the specimen.

The EF-TEM experiments were performed using a Philips CM30 (300 kV) TEM, equipped with a Gatan image-filtering (GIF) system that allows both parallel-detection EELS and energy-selected imaging/diffraction. This TEM provides a high beam current needed for chemical imaging. On the other hand, high current can introduce significant radiation damage to the specimen. However, it is rather surprising that the long-chain thiolate molecules were very robust under the high-energy electron beam, allowing stable imaging to be obtained. The threshold ionization energy of carbon is 284 eV, and the width of the energy window was controlled to be 20 eV to ensure the signal intensity.

The Ag nanocrystals were synthesized using an aerosol technique reported previously.[11−13] Briefly, an aerosol of unprotected nanoparticles was produced by evaporating bulk silver into a flowing carrier gas stream and slowly cooling it in an aggregation cell. Ultrahigh purity helium carried the silver vapor through a cooling region where nucleation of the nanocrystals took place. The emerging nanocrystal aerosol was then immediately diluted with a secondary helium stream, during which the dilution stream is added with an appropriate passivating or etching agent *n*-(dodecanethiol), so-called C_{12} thiolates, which have a fully extended chain length of 1.8 nm. The material was then dissolved in toluene and went through several cleaning stages using ethanol to rid the sample of excess thiol. TEM specimens were prepared by depositing a highly concentrated drop of the toluene solution onto an ultrathin amorphous SiO_x film substrate, which was chosen specifically for the chemical imaging to be described in the next section. Nanocrystal superlattices appear on the substrate film, in the form of highly oriented thin crystalline films.

3. Interparticle Molecular Bonding

We first show the observation of NCSs using conventional bright-field TEM. Figure 2 is a series of TEM images acquired

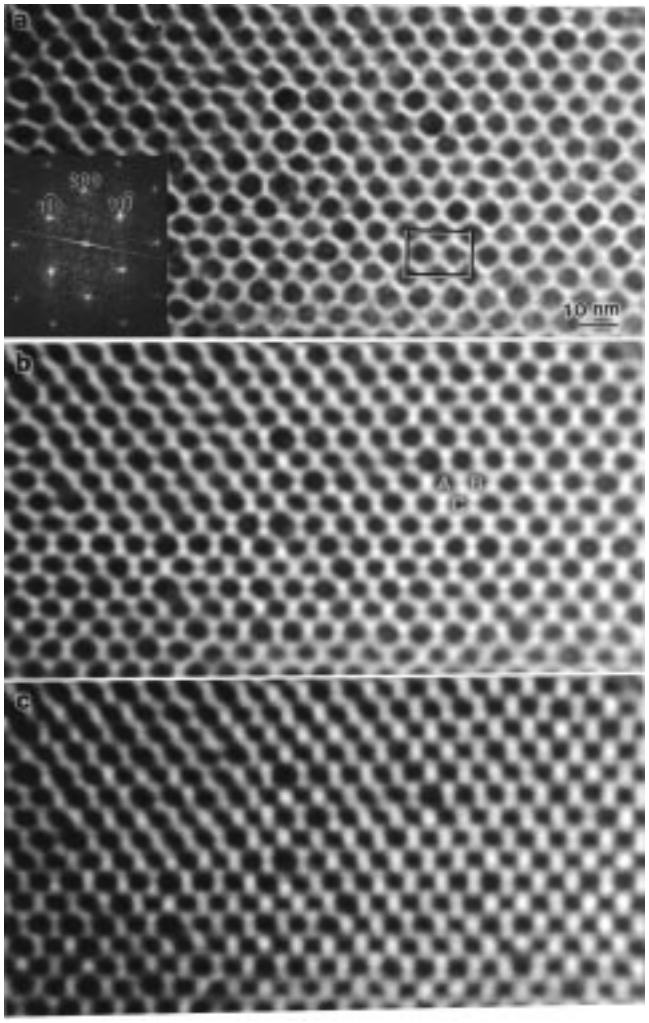

Figure 2. $[110]_s$ TEM images of self-assembled Ag NCSs recorded at (a) near in-focus, (b) under-focus, and (c) far under-focus. The NCS has the fcc packing structure of the multilayer superlattices with a lattice constant of $a_s = 10.5 \pm 0.3$ nm. The inset in (a) is a Fourier transform of the image and it is indexed as $[110]_s$ of fcc. The center-to-center interparticle distance is $d = a_s/\sqrt{2} \approx 7.5$ nm; thus, the core size is 5.5 nm after subtracting the face-to-face distance (2 nm) between the adjacent particles.

from the same area of the specimen under different defocus conditions. The crystal structure of the NCSs has been determined previously.[11−14] The projection of the unit cell is represented by a rectangle, which is the $[110]_s$ projection of a face-centered cubic lattice, where the subscript s refers to the Miller indexes of the superlattice. The geometrical shape of the nanocrystals is more easily seen in the images recorded at near-focus condition (Figures 2a). The NCSs are dominantly comprised of truncated octahedral Ag nanocrystals with {100} and {111} facets. The image recorded at the out-focus condition exposes a netlike pattern of directional "bonds" among neighboring nanocrystals (Figure 2b), where the bright spots between the nanocrystals may correspond to the lower-density channels between the bunched adsorbed molecules. Assembling of truncated octahedral nanocrystals usually starts with the $(110)_s$ plane of the fcc lattice, as proven by the diffractogram of the image shown in the inset of Figure 2a. This is an optimal orientation for imaging the adsorbed molecules on the nanocrystal surface because the nanocrystals are separated at the largest possible distance along one direction.

Self-assembled NCSs can form platelet "two-dimensional" structures as well as three-dimensional bulk crystals (Figure 3).

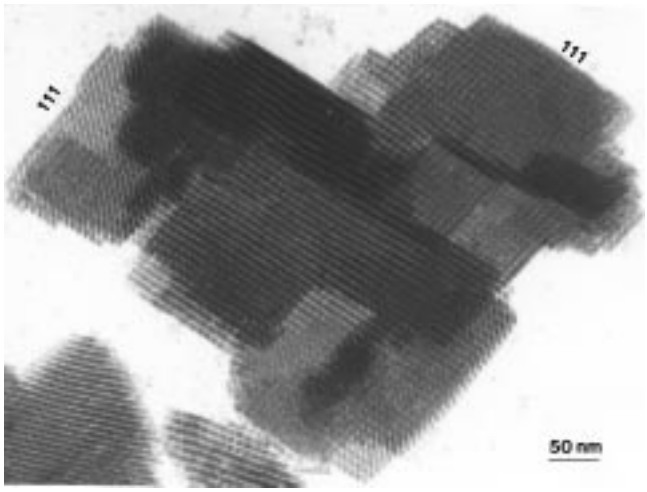

Figure 3. Three-dimensional, faceted superlattice assembly of Ag nanocrystals.

The bulk crystals usually have {111} facets possibly because of the most dense packing of the nanocrystals in the plane, resulting in lower surface energy. This phenomenon simply indicates the role played by surface energy in forming self-assembled superlattices and the strong interaction among the adsorbed molecules. At the atomic level, the {111} packing is usually preferred in close-packed structure because of the largest possible number of nearest neighbors. The similarity between NCSs and atomic lattice simply demonstrates the strong interaction between nanocrystals, which is mediated by the adsorbed thiolates.

To directly image the thiolate molecules distributed between the nanocrystals, EF-TEM is reliable and precise since the image contrast is directly proportional to the thickness-projected elemental density. Shown in Figure 4a is a bright field TEM image of a NCS, and the corresponding energy-filtered TEM image using the carbon K edge is given in Figure 4b. The shape of the nanocrystals is best revealed by high-resolution TEM (inset in Figure 4a). The nanocrystals are oriented at [110], along which two {100} facets and four {111} facets are projected edge-on. The EF-TEM image gives some interesting contrast features, and the projected carbon density between the particles shows a contrast pattern that is the strongest between the A and B types of particles, while the contrast is lower between the A and C or B and C types of particles. This contrast behavior is best seen by taking a line scan of the image intensity as indicated in Figure 4b, and the result is displayed in Figure 4c.

The contrast pattern observed in Figure 4b is a rather general feature of the energy-filtered TEM image of the NCSs using the carbon K ionization edge. Figure 5 shows an EF-TEM image of a relatively large area of the NCS. The rectangular represents the projected unit cell of fcc. The image intensity is the strongest between the A and B types of particles along $[1\bar{1}0]_s$. This is a unique evidence for constructing the molecular bonding model of the NCSs to be given below.

The nanocrystals we are interested in are dominated by truncated octahedra (Figure 6a), which has six {100} facets and eight {111} facets. The thiolate adsorbed headgroups (S-atoms) are assumed to be uniformly distributed on the facets of the nanocrystals (Figure 6b) and may be "bunched" by extending normal to the nanocrystal facet. The orientational relationship between the nanocrystal core's lattice and the superlattice has been established previously[11] as [110] || $[110]_s$ and [002] || $[1\bar{1}0]_s$. The $[110]_s$ projection of the NCS is schematically given

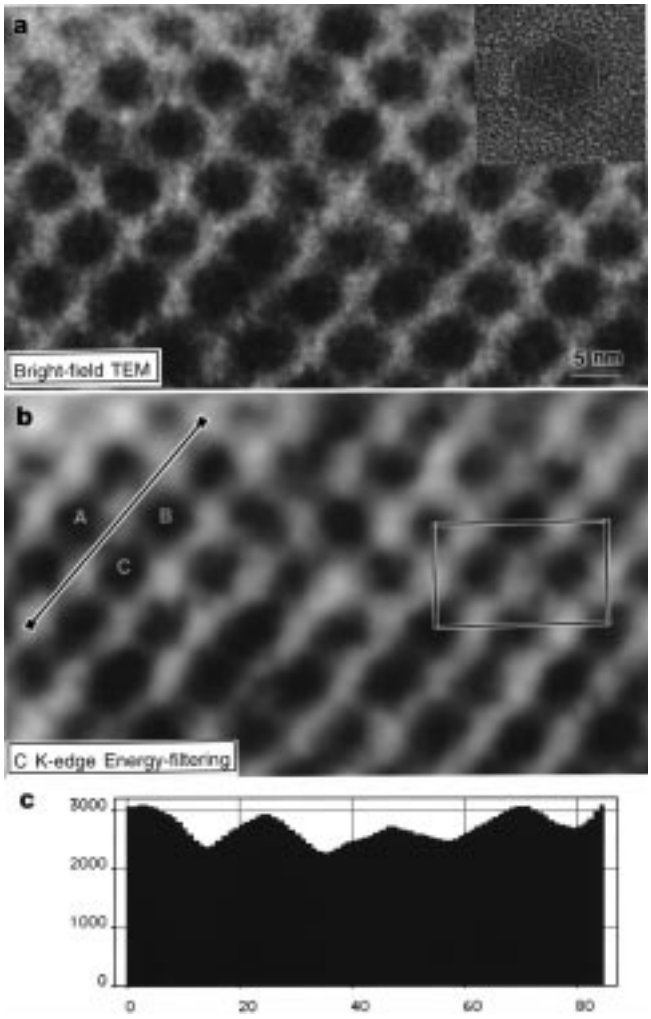

Figure 4. (a) $[110]_s$ bright-field TEM image and (b) energy-filtered TEM image of the carbon K ionization edge, showing the projected density of carbon atoms along the $[110]_s$ of the NCS. (c) Intensity profile along the line scan in (b).

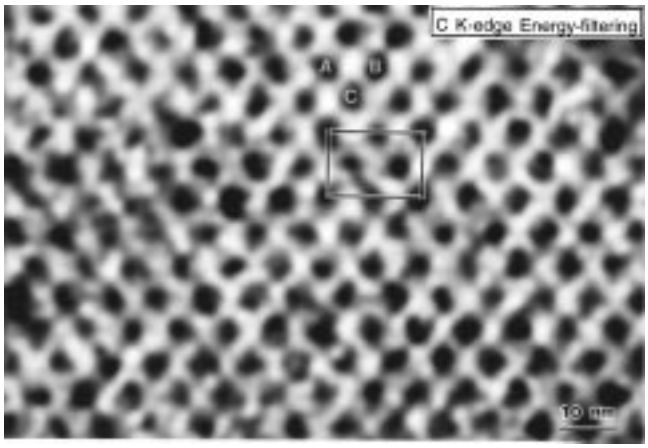

Figure 5. $[110]_s$ energy-filtered TEM image of the carbon K ionization edge, showing the projected density of carbon along the $[110]_s$ of the NCS.

in Figure 6c, where the gray nanocrystals are located at a layer of $z = a_s/\sqrt{2}$ above (out of plane) the first layer, where a_s is the lattice constant of the NCS. On the basis of the adsorbate structure model of Figure 6b, in which the thiolate chains from each facet are assumed to be codirected and tightly bunched, the corresponding chain-packing structure in the NCS is given in Figure 6c. From the image shown in Figure 2a, the face-

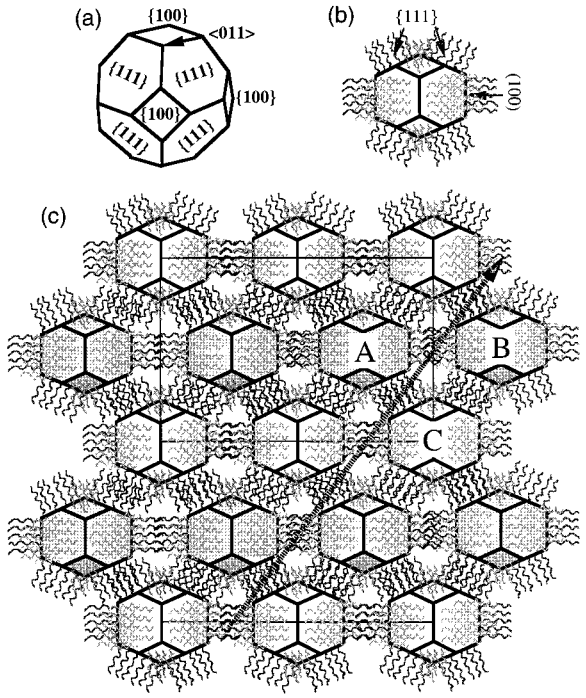

Figure 6. (a) Diagram of the truncated octahedron morphology of the Ag nanocrystals, with the {111} and {100} facet structure and ⟨011⟩ direction designated. (b) [110] projection of the TO nanocrystal with adsorbates. (c) $[110]_s$ projection of the NCS model, showing the distribution of passivated molecules between the nanocrystals. The projected unit cell is represented by a rectangle.

to-face distance between {100} facets of the two neighboring nanocrystals is 1.5−2.0 nm, while the length of the thiolate molecules is 1.8 nm; thus, there must be interdigitation among the adsorbed thiolates distributed on the surfaces of two adjacent nanocrystals. The face-to-face assembling of the nanocrystals also supports this interdigitation model. With the model shown in Figure 6c, a "channel" of low chain density is formed among three nanocrystal rows, in agreement with the image shown in Figure 2b.

We consider the projected density of the carbon chains. Three rows of nanocrystals labeled with A, B, and C are assigned for the convenience of our discussion. Nanocrystals A and C are assembled by arranging the {111} faces toward each other; thus, the carbon density between the particles is contributed mainly by the thiolate molecules adsorbed on the two {111} edge-on faces. The nanocrystals A and B are assembled by facing the {100} faces; in addition to the carbon density contributed by the interdigitated thiolates adsorbed on the {100} faces (viewed edge-on along $[110]_s$), the thiolates adsorbed on the four {111} planes (not edge-on) also contribute to the projected carbon density although the {111} faces are at an angle with the projection direction. Therefore, the projected density of the thiolate molecules between particles A and B is expected to be higher than that between A and C (or B and C) if the size of {111} faces is the same as that of {100} and the density of the adsorbed thiolate chains is the same on both {111} and {100}. This agrees with the experimental data shown in Figures 3b and 4. On the other hand, with consideration that the resolution of the EF-TEM is ∼2 nm, the channels formed by the bunched thiolates may not be well-resolved in these types of images. Therefore, the intensity line scan in the carbon elemental map (following the arrowhead) would give the profile displayed in Figure 4c, in which the peaks correspond to the thiolates distributed between the A and B types of particles and the valleys are the A and C (or B and C) interspacing.

4. Conclusion

In this paper, bundling and interdigitation of thiolate molecules adsorbed on Ag nanocrystals have been observed using the chemical imaging of energy-filtered transmission electron microscopy. In these orientationally ordered, self-assembled Ag−nanocrystal superlattices, the bunching adsorbates between facets of Ag cores is the foundation for the geometrical assembling of truncated octahedral nanocrystals. Further, many of the defects observed in the system can be interpreted on the basis of this structural principle.[14] A model consistent with the nanocrystal's geometry and bonding (polyhedral shapes and the bundling of adsorbates) has been proposed to account for the principal structure.

The result proves the molecular dynamic calculations of Luedtke and Landman,[15] who showed the bundling of long-chain thiolates on nanocrystal surfaces. The interdigitation of adsorbed chain molecules has also been indicated by the study of Alvarez et al.,[16] who used mass spectrometry to measure the core size of Au particles and X-ray diffraction to measure the interparticle distance. For ordered crystalline NCS structures, our result support the interdigitative interpenetration of the adsorbates distributed on the neighboring nanocrystals. For NCSs containing twinned structures, the "gear"-type assembling of bunched thiolates is required to interpret the rotation of the nanocrystals at the twin boundary.[14]

Acknowledgment. The authors thank Dr. I. Vezmar for kindly providing the specimens used in this study. Thanks also goes to Professor U. Landman for stimulating discussions. Research was partially sponsored by NSF Grant DMR-9632823 and by the Division of Materials Sciences, U.S. Department of Energy, under Contract DE-AC05-96OR22464 with Lockheed Martin Energy Research Corp., and through the SHaRE Program under Contract DE-AC05-76OR00033 with Oak Ridge Associated Universities.

References and Notes

(1) Murray, C. B.; Kagan, C. R.; Bawendi, M. G. *Science* **1995**, *270*, 1335.

(2) Whetten, R. L.; Khoury, J. T.; Alvarez, M. M.; S. Murthy, S.; I. Vezmar, I.; Wang, Z. L.; Cleveland, C. C.; Luedtke, W. D.; Landman, U. *Adv. Mater.* **1996**, *8*, 428.

(3) Andres, R. P.; Bein, T.; Dorogi, M.; Feng, S.; Henderson, J. I.; Kubiak, C. P.; Mahoney, W.; Osifchin, R. G.; Reifenberger, R. *Science* **1996**, *273*, 1690.

(4) Yin, J. S.; Wang, Z. L. *Phys. Rev. Lett.* **1997**, *79*, 2570; *J. Phys. Chem.* **1997**, *101*, 8979.

(5) Alvarez, M. M.; Khoury, J. T.; Schaaff, G.; Shafigullin, M. N.; Vezmar, I.; Whetten, R. L. *Chem. Phys. Lett.* **1997**, *266*, 91.

(6) Collier, C. P.; Saykally, R. J.; Shiang, J. J.; Henrichs, S. E.; Heath, J. R. *Science* **1997**, *277*, 1978.

(7) See: *Energy-Filtering Transmission Electron Microsocpy*; Reimer, L., Ed.; Springer Series in Optical Sciences 71; Springer: Berlin, 1995.

(8) Wang, Z. L.; Shapiro, A. J.*Ultramicroscopy* **1995**, *60*, 115.

(9) Krivanek, O. L.; Gubbens, A. J.; Dellby, N. *Microsc., Microanal., Microstruct.* **1991**, *2*, 315.

(10) Wang, Z. L. *Elastic and Inelastic Scattering in Electron Diffraction and Imaging*; Plenum Press: New York, 1995; Chapter. 6.

(11) Harfenist, S. A.; Wang, Z. L.; Alvarez, M. M.; Vezmar, I.; Whetten, R. L. *J. Phys. Chem.* **1996**, *100*, 13904.

(12) Harfenist, S. A.; Wang, Z. L.; Alvarez, M. M.; Vezmar, I.; Whetten, R. L. *Adv. Mater.* **1997**, *9*, 817.

(13) Alvarez, M. M.; Vezmar, I.; Whetten, R. L. *J. Aerosol Sci.*, in press.

(14) Wang, Z. L. *Adv. Mater.* **1998**, *10*, 13.

(15) Luedtke, W. D.; Landman, U. *J. Phys. Chem.* **1996**, *100*, 13323.

(16) Alvarez, M. M.; Khoury, J. T.; Schaaff, G.; Shafigullin, M. N.; Vezmar, I.; Whetten, R. L. *J. Phys. Chem. B* **1997**, *101*, 3706.